Drug Design, Development and Therapy

Dovepress
open access to scientific and medical research

Open Access Full Text Article

ORIGINAL RESEARCH

Novel synthesizing method of pH-dependent doxorubicin-loaded anti-CD22-labelled drug delivery nanosystem

This article was published in the following Dove Press journal:
Drug Design, Development and Therapy
7 September 2015
Number of times this article has been viewed

Mengjiao Sun[1,*]
Jun Wang[1,*]
Qin Lu[1]
Guohua Xia[2]
Yu Zhang[3]
Lina Song[3]
Yongjun Fang[1]

[1]Department of Hematology/Oncology, Nanjing Children's Hospital, Nanjing Medical University, [2]Department of Hematology, Zhongda Hospital, Medical School, Southeast University, [3]State Key Laboratory of Bioelectronics, Southeast University, Nanjing, People's Republic of China

*These authors have contributed equally to this work

Abstract: The objective of this study was to investigate the anticancer efficacy of dimercaptosuccinic acid-modified iron oxide magnetic nanoparticles coloaded with anti-CD22 antibodies and doxorubicin (anti-CD22-MNPs-DOX) on non-Hodgkin's lymphoma cells. The physical properties of anti-CD22-MNPs-DOX were studied and its antitumor effect on Raji cells in vitro was evaluated using the Cell Counting Kit-8 assay. Furthermore, cell apoptosis and intracellular accumulation of doxorubicin were determined by flow cytometry. The results revealed that anti-CD22-MNPs-DOX inhibited the proliferation of Raji cells, significantly increased the uptake of doxorubicin, and induced apoptosis. Therefore, it was concluded that a coloaded antibody and chemotherapeutic drug with magnetic nanoparticles might be an efficient targeted treatment strategy for non-Hodgkin's lymphoma.

Keywords: doxorubicin, anti-CD22 antibody, drug delivery system, target selection, non-Hodgkin lymphoma

Introduction

Malignant lymphoma, originating from lymphocyte ontogenesis and classified by pathologies and clinical characteristics, includes Hodgkin's lymphoma and non-Hodgkin's lymphoma (NHL), with the latter accounting for approximately 90% of all lymphomas.[1–3] Cancer statistics from the American Cancer Society for 2015 have shown that the incidence of NHL ranks fifth as the most common cancer in humans and accounts for 3.5% of all cancer-related deaths.[4] In particular, NHL (including Burkitt lymphoma) is the fourth most common type of cancer in children,[5] and the total 5-year relative survival rate was 84% from 2004 to 2010. Nevertheless, nearly 20% of patients still relapse within a year from diagnosis and go on to have a poor prognosis.[6] Owing to hematopoietic stem cell transplantation, treatment of refractory lymphoma has been greatly improved over the last few decades;[7] however, chemotherapy still prevails in lymphoma treatment, despite serious side effects, such as vomiting, bone marrow supression, and fatal infections. Thus, new therapeutic strategies with less toxicity and more efficiency are urgently needed for NHL.

Molecular targeted therapy has recently emerged as one of the most efficient antitumor therapies, and includes rituximab and dasatinib. which are used in the treatment of CD20-positive NHL[8,9] and Ph chromosome-positive chronic myeloid leukemia,[10,11] respectively. As we know, the majority of NHLs originally express B-lineage cell antigens, including CD19, CD20, and CD22.[12] Rituximab, a humanized monoclonal anti-CD20 antibody combined with the CHOP (cyclophosphamide, vincristine, doxorubicin, and prednisone) regimen, has not only improved overall and

Correspondence: Yongjun Fang
Department of Hematology/Oncology, the Affiliated Nanjing Children's Hospital of Nanjing Medical University, 72 Guangzhou Road, Nanjing, 210008, People's Republic of China
Tel +86 189 5176 9586
Fax +86 189 5176 9586
Email fyj322@189.cn

complete response rates, but also prolonged progression-free and overall survival rates in patients with CD20-positive NHL.[13] However, some patients undergoing treatment with anti-CD20 antibodies previously still went relapse and revealed less sensitivity to subsequent chemotherapy, leading to a tough problem for further chemotherapeutic treatment.[14] Expressed on the majority of normal and malignant B-lineage cells, CD22 has attracted much interest because of its receptor-mediated internalization. Humanized anti-CD22 antibodies were developed to minimize immunogenicity and enhance the interactions of effects during diagnosis and treatment systemic lupus erythematosus.[15] Preclinical tests with anti-CD22 antibodies indicated that a single, conjugated, or radiolabelled agent had antitumor activity in patients with recurrent and refractory NHL.[16,17] Importantly, it has been reported that anti-CD22 antibodies are well tolerated and have good therapeutic effects when used in combination with other agents. Therefore, there has been great interest in identifying and developing novel anti-CD22 drugs.

In recent decades, nanoparticles have been widely explored as drug carriers to minimize systemic side effects and to maximize the efficacy of chemotherapy. Owing to their nanometer diameter, stable physical properties, lack of cytotoxicity, and ability to enhance drug accumulation in cells, various types of nanomaterials, including magnetic nanoparticles (MNPs), liposomes, polymers, and microbubbles, have been investigated in depth for medical application.[18–20] One of the popular MNP drug delivery systems, Fe_3O_4 nanoparticles, exhibit a high drug-loading ratio and fewer dose-related side effects, and remain in the circulatory system for longer without being taken up by the reticuloendothelial system, making them excellent candidates for targeted drug delivery, as demonstrated by our previous studies showing that Fe_3O_4 nanoparticles loaded with chemotherapeutic drugs have enhanced targeted efficiency against cancer cells.[21,22]

In this work, we designed a novel and effective strategy for synthesizing a pH-dependent nanodrug delivery system, ie, doxorubicin-loaded anti-CD22-labelled MNPs (anti-CD22-MNPs-DOX), to enhance lymphoma targeting and cytotoxicity enhance lymphoma targeting and cytotoxicity in NHL. To our knowledge, no research on anti-CD22 antibodies linked to magnetic particles has been reported so far. Moreover, we applied the Fe^{2+}-DOX complex in a pH-dependent manner to improve drug release in tumor cells. Understanding the mechanism of action of anti-CD22-MNPs-DOX will help us design better anticancer drugs. Thus, the cell inhibition rate, intracellular concentration of doxorubicin, and apoptotic rate in NHL cells were assessed in vitro to estimate the efficiency of transport of doxorubicin into these cells. To our knowledge, there have been no reports of anti-CD22 antibodies being successfully attached to MNPs and doxorubicin.

Materials and methods

Main chemicals

Dimercaptosuccinic acid (DMSA)-modified MNPs were obtained from the Jiangsu Key Laboratory for Biomaterials and Devices (Southeast University, Nanjing, People's Republic of China). Roswell Park Memorial Institute 1640 medium containing 10% (v/v) heart-inactivated fetal calf serum for cell culture was purchased from Gibco (Omaha, NE, USA). Doxorubicin was purchased from Zhejiang Haizheng Pharmaceutical Co Ltd (Zhejiang Province, People's Republic of China). Cell Counting Kit-8 (CCK-8) was purchased from Donjindo Laboratories (Tokyo, Japan). The apoptosis detection kit and 4′,6-diamidino-2-phenylindole (DAPI) were obtained from KeyGen Biotech Co Ltd (Nanjing, People's Republic of China), and the anti-CD22 antibody was supplied by Santa Cruz Biotechnology (Santa Cruz, CA, USA). All other reagents were of analytical grade. All experiments were evaluated and approved by the Animal and Ethics Review Committee of Nanjing Medical University (Nanjing, Jiangsu Province, China).

Preparation of anti-CD22-MNPs

Iron oxide nanoparticles primarily modified by DMSA were supplied by Jiangsu Key Laboratory for Biomaterials and Devices.[23] The antibodies were connected to the MNPs using EDC/NHS methods.[24] An acylation reaction was conducted between the activated carboxyl groups and the amino terminals of the antibodies for 24 hours. Briefly, DMSA-MNPs were reactive with EDC/NHS followed by addition of anti-CD22 antibodies (mass ratio of Fe to anti-CD22 1 mg:300 μg) with constant shaking overnight at room temperature. The anti-CD22-MNPs were purified using an S-300 polyacrylamide gel column to remove unlinked antibody. The eluent was collected to calculate the amount of antibody by Bradford assay. Meanwhile, gel stained with Coomassie Brilliant blue R-250 was used to visualize the protein bands of the anti-CD22 antibody with and without MNPs. The anti-CD22-MNPs were then harvested by centrifugation at 3,000× *g* for 10 minutes at 4°C, and used immediately after washing twice with ice-cold phosphate-buffered saline (pH 7.4).

Preparation of DOX-Fe^{2+} complex and anti-CD22-MNPs-DOX

The DOX-Fe^{2+} complex was prepared by adding sufficient $FeSO_4$ into a doxorubicin solution, (1.5 M excess of Fe^{2+} over doxorubicin) followed by incubation with anti-CD22-MNPs

in the dark for 15 minutes.[25,26] KOH was added to the solution in an amount sufficient to maintain the pH at around 7.4. The drug-loaded MNPs were harvested by centrifugation at 15,000× *g* for 30 minutes at 4°C to remove the excess doxorubicin. Finally, the anti-CD22-MNPs-DOX precipitate was washed and dispersed with ice-cold phosphate-buffered saline (pH 7.4) and used immediately.

Characterization of MNPs

The morphology of the nanoparticles was analyzed by transmission electron microscopy (JEM-2100; JEOL, Tokyo, Japan) and the hydrodynamic diameter was measured by dynamic light scattering (Nano ZS90; Malvern Instruments, Westborough, MA, USA). The zeta potential of these materials when dissolved in deionized water was determined using a Zeta Plus analyzer (Brookhaven Instruments, Holtsville, NY, USA).

Determination of drug loading

In this paper, we applied the DOX-Fe^{2+} complex by adding doxorubicin into $FeSO_4$ solution, as intermediates to connect doxorubicin to nanoparticles. It has been reported that the DOX-Fe^{2+} complex can dissolve completely within 15 minutes in acid solution.[27]

For determination of drug-loading, the weighed, freeze-dried drug-loaded MNPs were suspended in phosphate-buffered saline (pH 5.6) at 4°C for 30 minutes to stimulate complete release of doxorubicin and were then harvested by centrifugation at 12,000× *g* for 30 minutes at 4°C. The absorbance in the supernatant was then measured at 488 nm using an ultraviolet-visible spectrophotometer (UV-3600; Shimadzu, Tokyo, Japan). The drug concentration was calculated using a calibration curve. Percent drug loading was defined as the free weight of doxorubicin over the total weight of anti-CD22-MNPs-DOX.

Anti-CD22-MNPs-DOX drug release kinetics in vitro

To study the kinetics of the pH-activated nanoparticles, aliquots of anti-CD22-MNPs-DOX were placed in two dialysis membrane bags with a molecular weight cutoff of 8,000–14,000 Da, dispersed in phosphate-buffered saline (pH 7.4 or pH 5.6), followed by continuous shaking at 37°C. The amount of supernatant in the tube was analyzed at set time intervals using an ultraviolet-visible spectrophotometer and complemented with fresh buffer for next analysis.

Cell culture

A Raji (CD22-positive Burkitt lymphoma) cell line, purchased from the Type Culture Collection of the Chinese Academy of Sciences (Shanghai, People's Republic of China), was cultured in Roswell Park Memorial Institute 1640 medium containing 10% (v/v) fetal calf serum, 100 U/mL penicillin, and 100 μg/mL streptomycin at 37°C in a 5% CO_2 incubator and passaged every 2–3 days. Cells used in the experiments were in the logarithmic growth phase.

Cell inhibition assay

The cell inhibition rate was measured by CCK-8 assay in vitro. In brief, Raji cells were seeded in 96-well plates (2×10^4 cells per well) and exposed to different concentrations of doxorubicin solution (DOX-Sol), DOX-MNPs, or anti-CD22-DOX-MNPs after 4 hours. The doses of doxorubicin incorporated in the MNPs were equal to the corresponding concentration of DOX-Sol. Meanwhile, cells treated with Roswell Park Memorial Institute 1640 medium alone were used as the control. After incubation for 24 or 48 hours, 10 μL of CCK-8 was added to each well, followed by incubation for a further 3–4 hours. Optical density (OD) was read at 488 nm using a microplate reader (Multiskan MK3; Thermo Scientific, Boston, MA, USA). The cell inhibition rate was calculated as: $(1- OD_{\text{treated cells}}/OD_{\text{control cells}}) \times100\%$. Finally, dose-effect curves were constructed and the 50% inhibition rates and half maximal inhibitory concentration (IC_{50}) values were calculated.

Apoptosis assay

First, 2×10^5 Raji cells were exposed to DOX-Sol, DOX-MNPs, or anti-CD22-MNPs-DOX for 24 hours. After being stained with DAPI for 5 minutes and washed in phosphate-buffered saline three times, the cells were suspended with 500 μL of binding buffer and 5 μL of Annexin V-fluorescein isothiocyanate for 15 minutes. The apoptosis rates were then determined by FACSCalibur flow cytometry (BD Biosciences, San Jose, CA, USA) at excitation and emission wavelengths of 479 nm and 587 nm, respectively. The apoptosis rates were calculated as the sum of early apoptosis and late apoptosis.

Fluorescence intensity of intracellular doxorubicin

As described above, Raji cells were cultured, collected at a series of time points, and washed with phosphate-buffered saline three times. The fluorescence intensity (FI) of the intracellular doxorubicin was detected by flow cytometry at an excitation wavelength of 488 nm. The relative FI was calculated as $FI_{\text{treated cells}}/FI_{\text{control cells}}$.

Morphology of apoptosis

First, 2×10^5 Raji cells were seeded in a 6-well plate for 2 hours. DOX-Sol, MNPs-DOX, or anti-CD22-MNPs-DOX (containing an equal concentration of doxorubicin) was then added in. After incubation for 24 hours, the cells were collected, washed twice with phosphate-buffered saline, and stained with DAPI for 5 minutes. The morphological changes in the nuclei were then observed by laser confocal spectral imaging (LSM710; Zeiss, Oberkochen, Germany).

Statistical analysis

All experiments were performed in triplicate. The data are expressed as the mean ± standard deviation. Statistical analyses were performed using Statistical Package for the Social Sciences software (version 19.0; IBM SPSS Statistics for Windows, Version 19.0) using the Student's *t*-test. $P<0.05$ was deemed to be statistically significant.

Results

Characteristics of nanoparticles

The characteristics of MNPs and anti-CD22-MNPs-DOX were observed by transmission electron microscopy. As shown in Figure 1A, the MNPs had a quasi-spherical shape, with an average diameter of 7–10 nm. After modification with the antibody and doxorubicin, the average diameter of the anti-CD22-MNPs-DOX increased to 13–16 nm, with no obvious aggregation visible (Figure 1B). The mean hydrodynamic size of the MNPs was about 23 nm (Figure 1C), while that of the anti-CD22-MNPs-DOX was nearly 150 nm. This is due to the modification of doxorubicin and antibodies, and neither could be seen under transmission electron microscopy. Only the iron cores were captured, which explains why there is no significant difference between Figure 1A and B. The zeta potential of the MNPs, DOX-MNPs, and anti-CD22-MNPs-DOX was −24.8±3.6 mV, −15.7±2.9 mV, and −16.3±1.9 mV, respectively. There was also no significant difference in the zeta potential between anti-CD22-MNPs and anti-CD22-MNPs-DOX ($P>0.05$).

To allow sufficient doxorubicin to combine with the nanoparticles, the DOX-Fe^{2+} complex was applied as an intermediate to the surface of MNPs according to a previous study[27] and the mass ratio of the DOX-Fe^{2+} complex and the MNPs with and without the antibody ranged from 10% to 100%. The drug loading percentage is shown in Table 1.

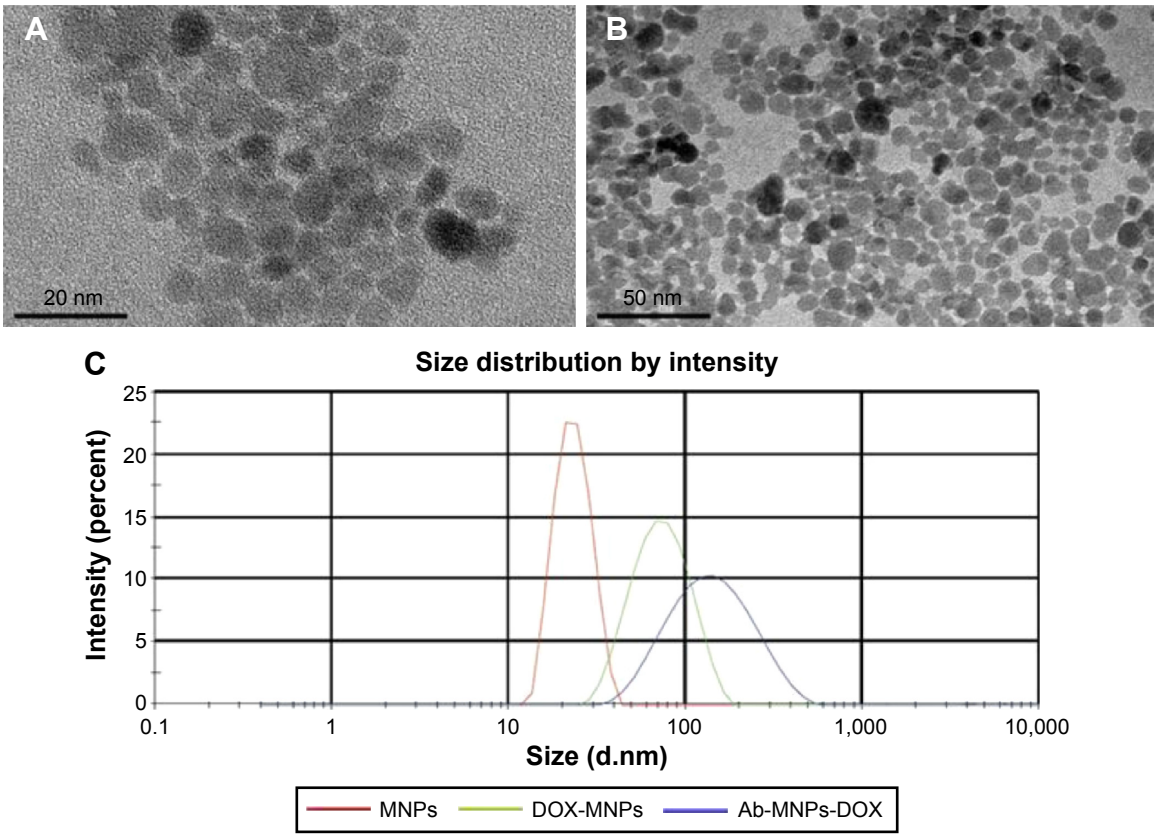

Figure 1 Characteristics of DMSA-MNPs (**A**), anti-CD22-MNPs-DOX (**B**), and particle size distribution (**C**) under electron microscopy.
Abbreviations: Ab, antibody; DMSA, dimercaptosuccinic acid; DOX, doxorubicin; MNPs, magnetic nanoparticles.

Table 1 Doxorubicin loading in anti-CD22-MNPs-DOX nanoparticles (mean ± standard deviation, n=3)

DOX-MNPs (% w/w)	Drug loading (% w/w)
10	8.93±1.91
20	17.43±2.85
100	12.47±2.05

Abbreviations: DOX, doxorubicin; MNPs, magnetic nanoparticles.

The increased drug loading was accompanied by an increase DOX-Fe^{2+} complex. The loading efficiency peaked when the added complex ratio was 20%, and this may have been attributable to the changes in surface potentials properties (data not shown). Based on the results for percent drug loading, a mass ratio of 20% was chosen to achieve maximum usage of doxorubicin in the following experiments.

Release of doxorubicin from the anti-CD22-MNPs in vitro was described for pH 5.6 and pH 7.4 at 37°C (Figure 2). Doxorubicin was released in the first 30 minutes at pH 5.6, with cumulative drug release reaching nearly 80% in 4 hours, followed by a plateau; at pH 7.4, drug release was stable and sustained for up to 48 hours.

The results of the Bradford assay showed that approximately 74% of the antibody was linked to the MNP surface, and this was also demonstrated by Coomassie Brilliant blue staining (Figure 3), indicating that the anti-CD22 antibody was successfully linked to the MNPs.

Antiproliferative activity

The MNPs alone had no obvious cytotoxic effect on Raji cells after treatment for 48 hours (Figure 4A); even the cell inhibition rate was still less than 5% when the concentration of MNPs was no more than 12.5 mg/L. After exposure to DOX-Sol, DOX-MNPs, or anti-CD22-MNPs-DOX for 24 or 48 hours, cell inhibition rates increased in a dose-dependent manner in all three groups (Figure 4B and C). The antiproliferative effects of chemotherapeutic drugs on tumor cells also occurred in a time-dependent manner. Briefly, when dealt with the same drug, the longer incubation time was, the higher the inhibition rate was, and the lower IC_{50} value was determined. It can be seen in Table 2 that the IC_{50} values at 48 hours are markedly lower than those at 24 hours, and that the IC_{50} values for anti-CD22-MNPs-DOX are significantly lower than those for DOX-Sol or MNPs-DOX (Table 2).

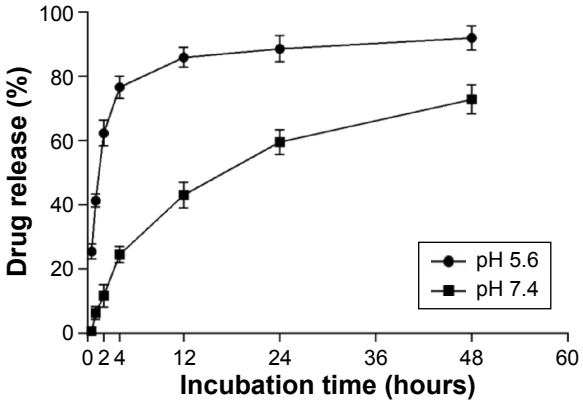

Figure 2 In vitro release of doxorubicin from anti-CD22-MNPs-DOX.
Notes: The drug release rate at pH 5.6 is significantly different from that at normal pH. And *P* values from statistics of the same line were <0.05.
Abbreviations: DOX, doxorubicin; MNPs, magnetic nanoparticles.

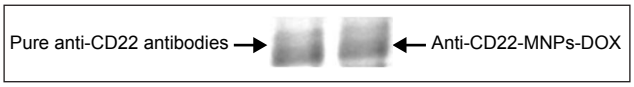

Figure 3 Protein bands of anti-CD22 with and without MNPs-DOX stained by Coomassie Brilliant blue R250.
Abbreviations: DOX, doxorubicin; MNPs, magnetic nanoparticles.

Apoptosis rate determined by flow cytometry

Apoptosis in Raji cells was 28.01%±2.39% for DOX-Sol, 10.97%±0.99% for DOX-MNPs, and 31.57%±4.27% for anti-CD22-MNPs-DOX (Figure 5), suggesting that the antiproliferative effect of anti-CD22-MNPs-DOX and DOX-Sol was significantly higher than that of DOX-MNPs ($P<0.05$).

Increased uptake of anti-CD22-MNPs-DOX in Raji cells

The FI of intracellular doxorubicin (as shown in Figure 6A) was determined by flow cytometry at 488 nm owing to the autofluorescence feature of doxorubicin, and the relative FI is shown in Figure 6B. The FI of intracellular doxorubicin in Raji cells increased in a time-dependent manner in all groups. Relative FI was much higher in the anti-CD22-MNPs-DOX group than in the DOX-MNPs and DOX-Sol group ($P<0.05$), suggesting that lymphoma targeting in CD22-overexpressing cells was improved by addition of anti-CD22 antibody to the MNPs. The FI of intracellular doxorubicin was also investigated in a CD22-negative leukemia T-cell (Jurkat) line. As described above, Jurkat cells were cultured with DOX-Sol, DOX-MNPs, and anti-CD22-MNPs-DOX for 6 hours and washed with phosphate-buffered saline three times; the relative FI (Figure 7) was 4.12±0.37, 4.53±0.29, and 4.85±0.66, respectively, with no significant increase in cellular uptake of doxorubicin seen in any of the treatment groups ($P>0.05$). Therefore, no antiproliferative studies were done using Jurkat cells.

The fluorescence of the doxorubicin-loaded nanoparticles when taken up by Raji cells was also visualized by laser confocal spectral imaging (Figure 8). The intracellular

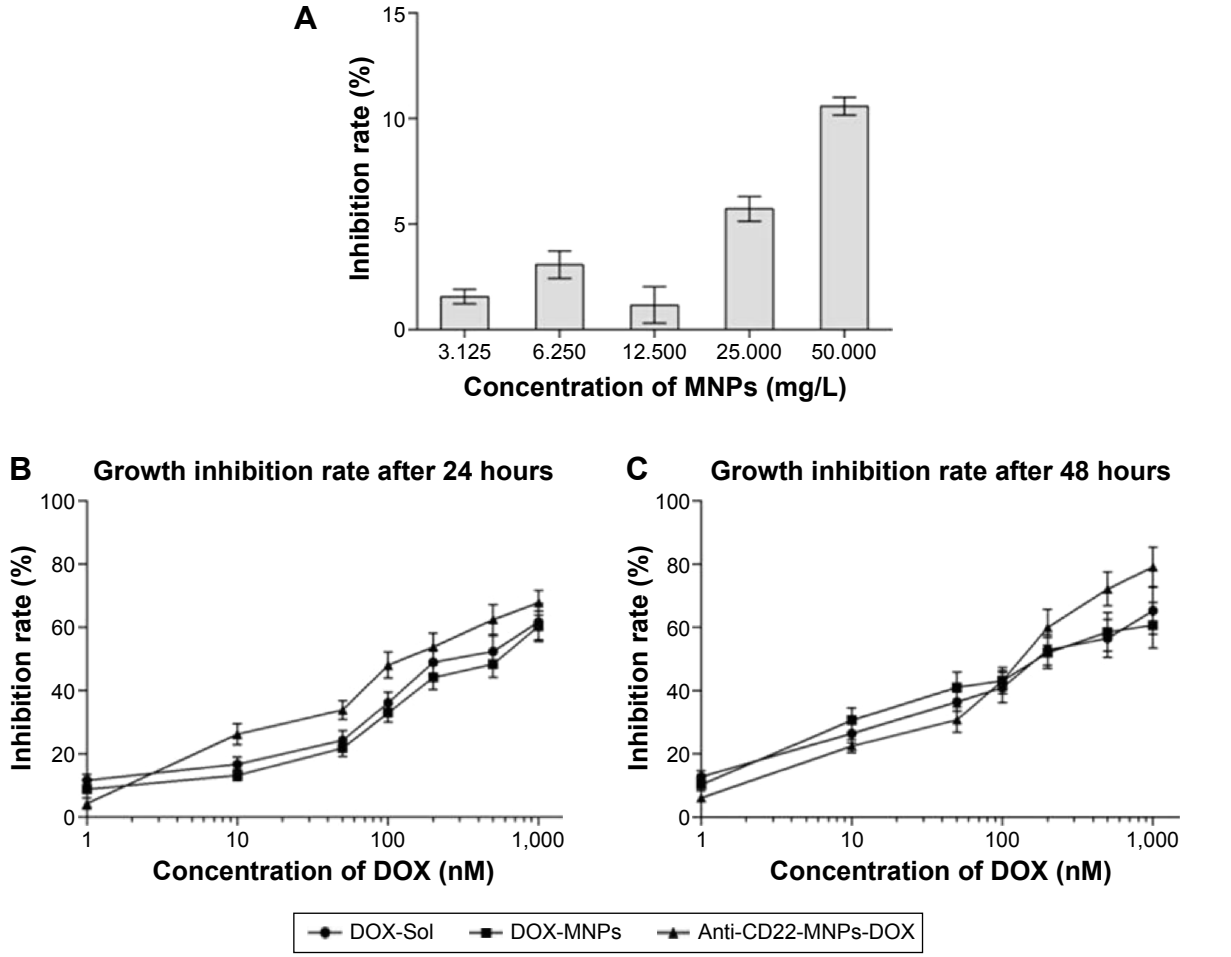

Figure 4 Cytotoxicity of MNPs (**A**), doxorubicin, DOX-MNPs, and anti-CD22-MNPs-DOX on Raji cells for 24 hours (**B**) and 48 hours (**C**) as determined by Cell Counting Kit-8 assay.
Abbreviations: DOX, doxorubicin; MNPs, magnetic nanoparticles; Sol, solution.

intensity of doxorubicin in the DOX-Sol group was seen mainly in the cytoplasm, with very little accumulation in cell nuclei. In contrast, an increase in doxorubicin intensity was evident in the nuclei (white arrows) of cells treated with anti-CD22-MNPs-DOX. Typical nuclear features of apoptosis (green arrows), such as chromatin condensation, fragmentation, and apoptotic bodies, could be seen easily in cells treated with anti-CD22-MNPs-DOX. These findings strongly suggest that our novel anti-CD22-MNPs-DOX formulation can improve the delivery of chemotherapeutic drugs to lymphoma cells and reinforce their antitumor effects.

Table 2 IC_{50} values for DOX-Sol, DOX-MNPs, and anti-CD22-MNPs-DOX at 24 and 48 hours (mean ± standard deviation, n=3)

IC_{50}	DOX (nM)	DOX-MNPs (nM)	Anti-CD22-MNPs-DOX (nM)
24 hours	339.23±23.33	495.21±30.04	156.32±28.78
48 hours	172.72±12.35	189.37±16.85	118.93±13.87

Abbreviations: DOX, doxorubicin; MNPs, magnetic nanoparticles; IC_{50}, half maximal inhibitory concentration; DOX-Sol, doxorubicin solution.

Discussion

Characterized by morphology (M), immunology (I), cytogenetic (C) and molecular (M), NHL can be divided into several series,[2] and due to the use of related short-term and intensive chemotherapy the outcomes of patients with NHL have been improved considerably. Further, short-term intensive chemotherapy has significantly increased overall survival in children and adolescents with NHL.[28,29]

For over 50 years, doxorubicin, a member of the CHOP regimen, has played an important role in the curative treatment of NHL. Doxorubicin exerts its antitumor effect by interfering with DNA, producing active oxygen radicals, and inducing apoptosis. In order to achieve better anticancer efficacy, high doses of doxorubicin were used in clinical trials, but resulted in serious side effects, including oral ulceration, cardiotoxicity, and myelosuppression. Therefore, much research interest has focused on how to improve tumor targeting while minimizing systemic side effects.

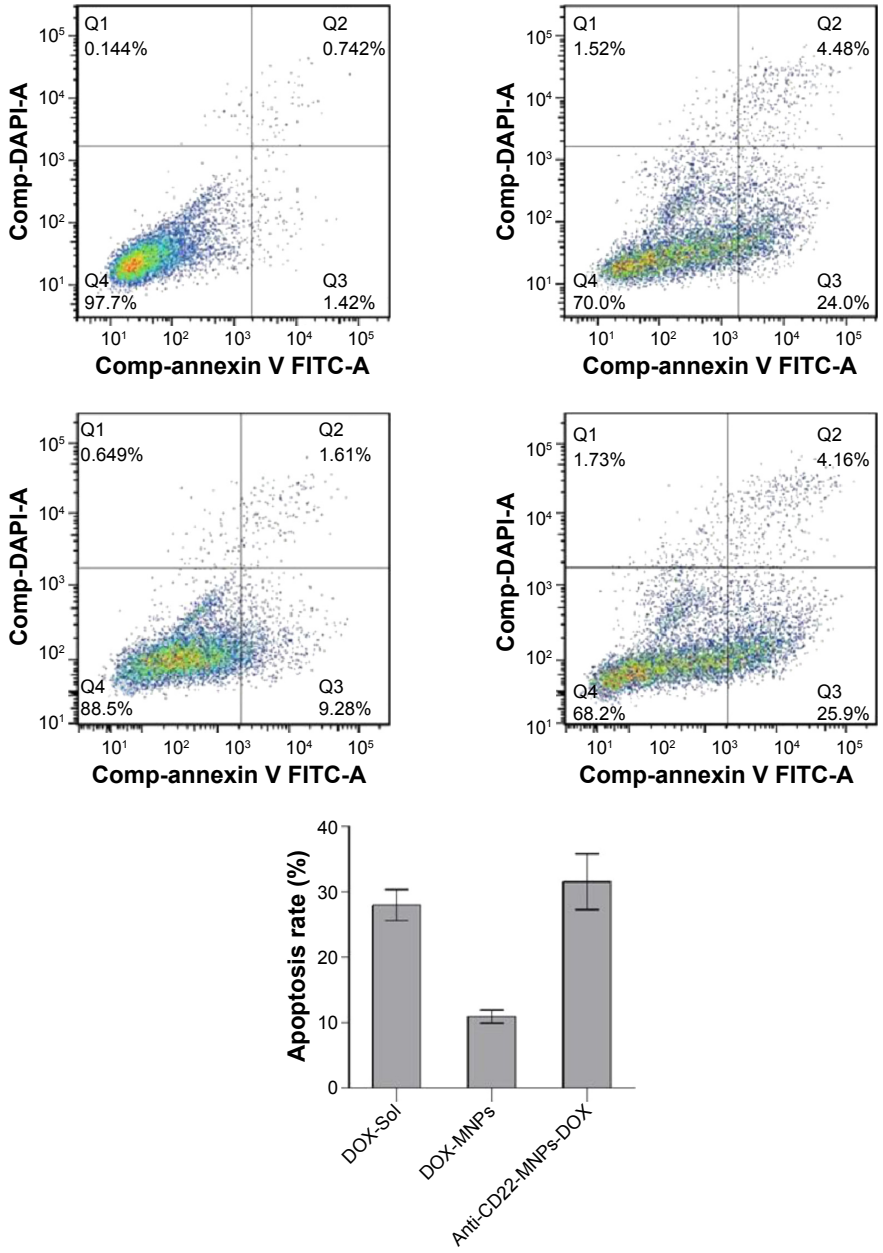

Figure 5 Apoptosis rates of Raji cells for 24 hours by flow cytometry.
Abbreviations: DAPI, 4′,6-diamidino-2-phenylindole; FITC, fluorescein isothiocyanate; DOX, doxorubicin; MNPs, magnetic nanoparticles; Sol, solution; Comp, compound.

Nanoparticle drug delivery systems are now a hot research topic because of their unique characteristics. MNPs have been widely studied and shown to be excellent contrast agents for early cancer diagnosis and targeted drug delivery.[30–32] Our previous studies have demonstrated the antitumor mechanisms of drugs combined with MNPs exerted cytotoxic effects by inducing apoptosis.[21,22] In this work, we synthesized a novel pH-dependent nanoparticle delivery system in which iron oxide cores are modified by DMSA to improve the nanoparticles aqueous dispersion. The hydrophilic surface of DMSA-MNPs also produces enough free carboxyl groups for further conjugation. It has been demonstrated the liposomal DOX used in the CHOP regimen achieves a 75% complete response rate. Further, PEGylated liposomal doxorubicin, when incorporated into the Rituximab plus CHOP (R-CHOP) regimen, had a complete release rate of 59% in elderly patients being treated for diffuse large B-cell lymphoma;[33] the liposome-encapsulated doxorubicin had an average diameter of 100 nm and showed excellent targeting, reduced cardiotoxicity, and increased drug concentrations in the targeted organs. In our present work, the average hydrodynamic diameter of anti-CD22-MNPs-DOX was 158±9.67 nm on dynamic light scattering analysis, which

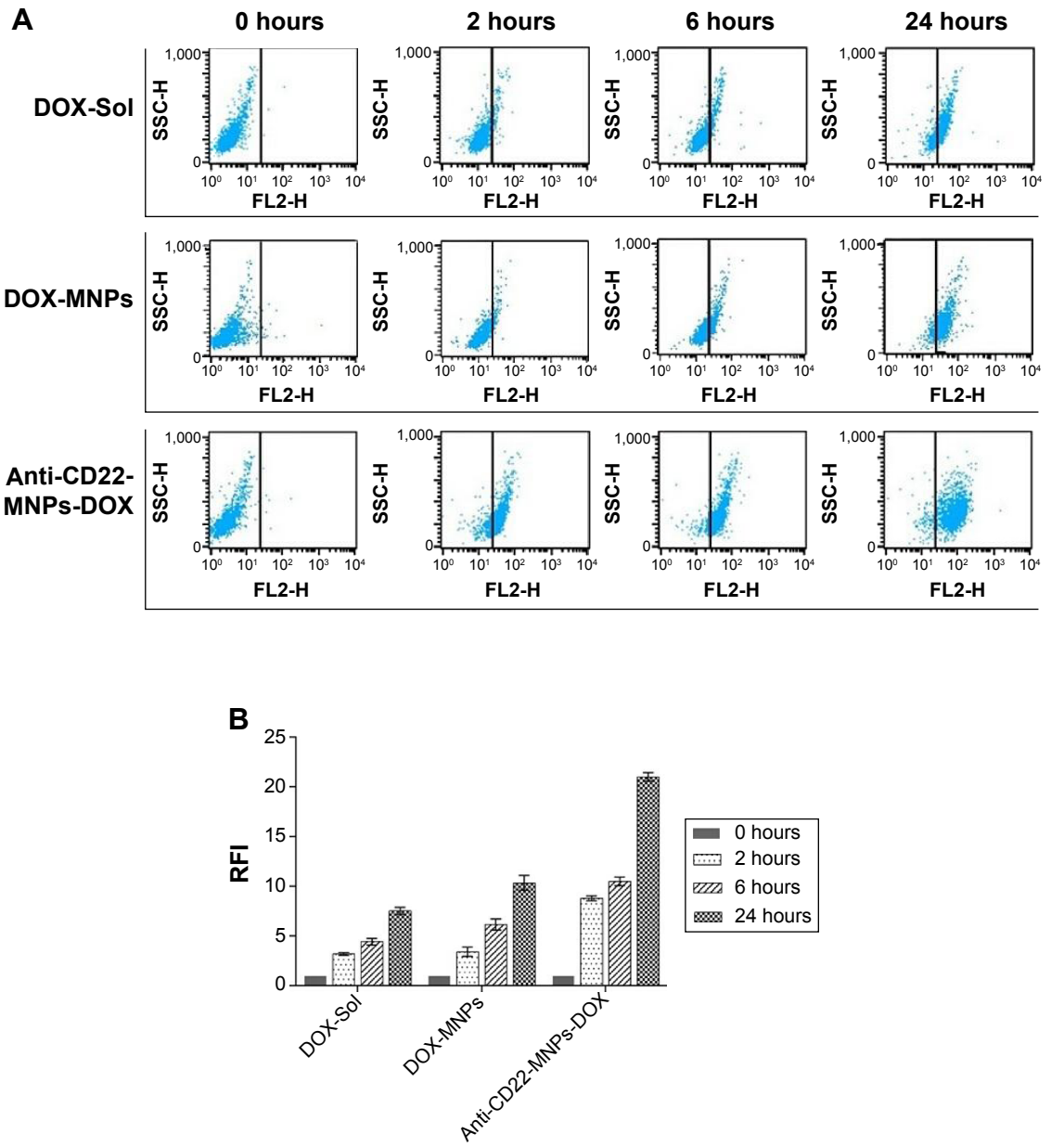

Figure 6 Intracellular accumulation of doxorubicin in Raji cells cultured with the different study formulations for various periods of time. The FI of intracellular doxorubicin (**A**) was determined by flow cytometry at 488 nm owing to the autofluorescence feature of doxorubicin, and the relative FI is shown in (**B**).
Abbreviations: DOX, doxorubicin; MNPs, magnetic nanoparticles; RFI, relative fluorescent intensity; Sol, solution.

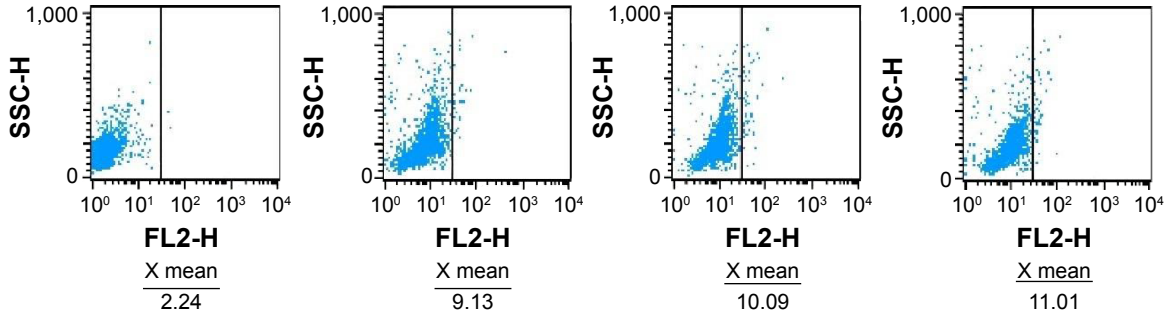

Figure 7 Intracellular accumulation of doxorubicin in Jurkat cells cultured with the different study formulations for 6 hours. X= the average RFI of doxorubicin in Jurkat cells.

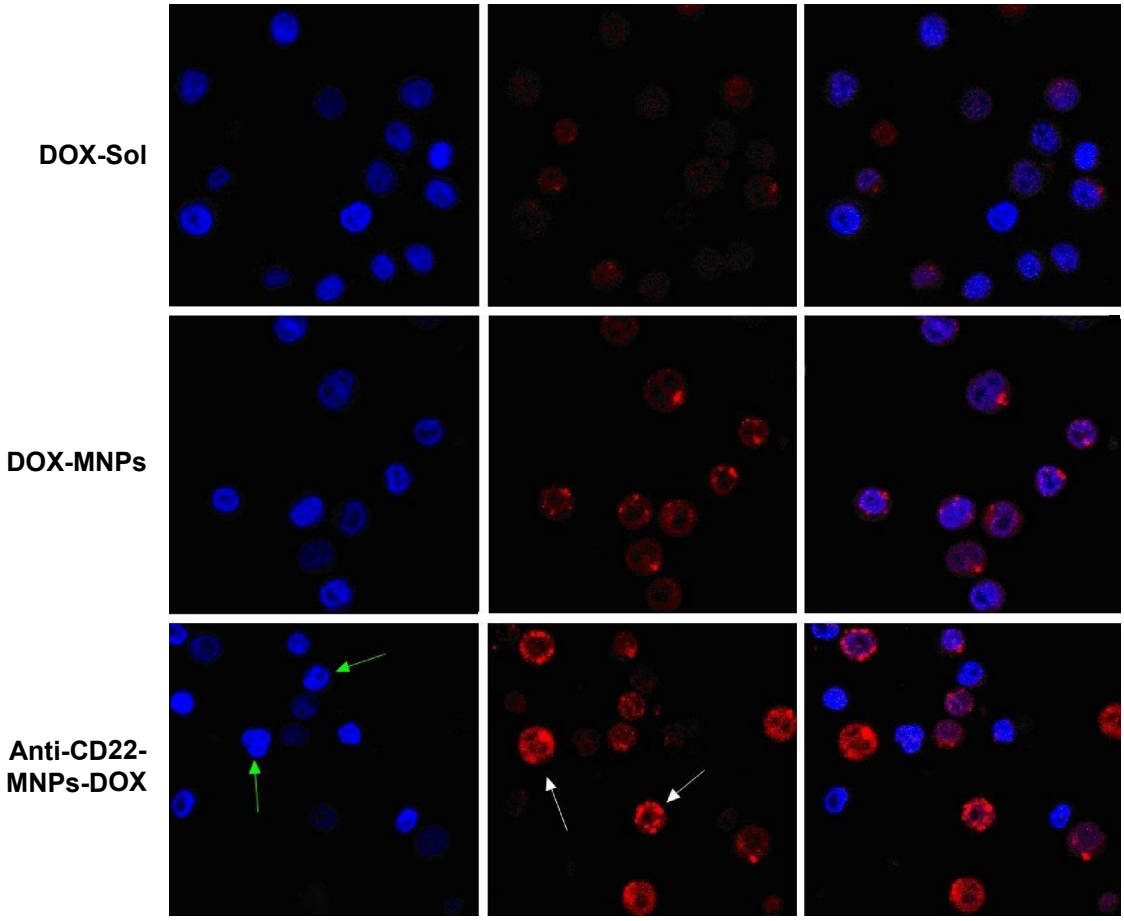

Figure 8 Morphological characterization of Raji cells by laser confocal spectral imaging (200×, DAPI). The signification of arrows shows the increased uptake of anti-cD22-MnPs-DOX in Raji cells. With the green arrows indicating the nuclei with blue fluorescence and white arrows indicate the cytoplasm with red fluorescence.
Abbreviations: DAPI, 4,6-diamidino-2-phenylindole; DOX, doxorubicin; MNPs, magnetic nanoparticles; Sol, solution.

was larger than that seen on transmission electron microscopy, and the zeta potential in water was −16.3±1.9 mV. Thus, we infer that the suitable size (<200 nm) of anti-CD22-MNPs-DOX grants it without being swallowed by reticular endothelial system or rapid renal excretion, thus allowing enough doxorubicin being taken by tumor cells through the enhancing the effect of permeation and retention.[34]

Compared with the report by Munnier et al[25] our formulation has a higher drug-loading ratio, in which the chemo-of-COOH groups in DMSA allow more combination sites for doxorubicin. Importantly, our present synthesis method does not rely on mechanical absorption, but chemical bound between surface connections, thus a stable sustained release over a prolonged period time within 48 hours can be seen at normalized pH situation in our present study. It has been documented that the pH of blood and normal tissue is neutral,[35,36] which strictly restricts the release of DOX-Fe^{2+} in our formulation. Interestingly, once the pH decreased to 5.6, the DOX-Fe^{2+} complex was completely dissociated within 15 minutes, which may be the reason why such rapid drug release was seen in the first 2 hours. According to another original research paper,[37] Fe^{2+} is bound to doxorubicin via the {C (11)-O^{-}; C (12)=O} chelating site, and the DOX-Fe^{2+} complex could be separated if surrounded by redundant H^{+} ions. When H^{+} ions were added into solution, the DOX-Fe^{2+} complex dissociated in just a few minutes. Since the relatively low pH in tumors inter-environment stimulates release of doxorubicin, pH-dependent anti-CD22-MNPs-DOX may be useful in the treatment of patients with NHL.

It is noteworthy that the antiproliferative effect of our novel anti-CD22-MNPs-DOX formulation is significantly higher than that of DOX-Sol or DOX-MNPs in terms of inhibition rate and apoptosis rate. The data in Figure 2 indicate that only about 80% of the loaded doxorubicin was released by 48 hours, owing to the sustained-release action of this formulation. This might provide an explanation for the comparatively low antitumor efficacy of DOX-MNPs. When anti-CD22 antibodies are linked to MNPs, they are taken up rapidly by cells with high CD22 expression, which significantly improves tumor-targeting efficiency. Further,

no obvious toxicity was seen in Raji cells, even when the MNP concentration was increased to rather high levels, suggesting that MNPs may be a safe drug delivery system. Our present findings suggest that this novel pH-dependent formulation is an effective drug delivery system for systemic administration.

Conclusion

The results of this study demonstrate that anti-CD22-MNPs-DOX has good aqueous dispersion properties, an appropriate hydrodynamic size, and efficient drug-loading ability, enables rapid drug release in an acidic environment, and has excellent antitumor efficiency. This novel formulation is a promising systemic chemotherapy for NHL and might be expanded for treatment of other cancers. Further research is needed to determine the antitumor effects and pharmacokinetics of this formulation in vivo, and the mechanism by which it induces apoptosis.

Acknowledgments

This work was supported financially by the National Nature Science Foundation of People's Republic of China (81201704) and the Science and Technology Development Funds Key Program of Jiangsu Province. We thank Dr Yu Zhang (National Laboratory of Molecular and Biomolecular Electronics, Southeast University) for providing technical assistance.

Disclosure

The authors report no conflicts of interest in this work.

References

1. Rademaker J. Hodgkin's and non-Hodgkin's lymphomas. *Radiol Clin North Am*. 2007;45:69–83.
2. Shankland KR, Armitage JO, Hancock BW. Non-Hodgkin lymphoma. *Lancet*. 2012;380:848–857.
3. Hennessy BT, Hanrahan EO, Daly PA. Non-Hodgkin lymphoma: an update. *Lancet Oncol*. 2004;5:341–353.
4. Siegel RL, Miller KD, Jemal A. Cancer Statistics, 2015. *CA Cancer J Clin*. 2015;65:5–29.
5. Ward E, DeSantis C, Robbins A, et al. Childhood and adolescent cancer statistics, 2014. *CA Cancer J Clin*. 2014;64:83–103.
6. Kim H, Park ES, Lee SH, et al. Clinical outcome of relapsed or refractory Burkitt lymphoma and mature B-cell lymphoblastic leukemia in children and adolescents. *Cancer Res Treat*. 2014;46:358–365.
7. Bhatt VR, Vose JM. Hematopoietic stem cell transplantation for non-Hodgkin lymphoma. *Hematol Oncol Clin N Am*. 2014;28:1073–1095.
8. Plosker GL, Figgitt DP. Rituximab: a review of its use in non-Hodgkin's lymphoma and chronic lymphocytic leukaemia. *Drugs*. 2003;63:803–843.
9. Harrison AM, Thalji NM, Greenberg AJ, et al. Rituximab for non-Hodgkin's lymphoma: a story of rapid success in translation. *Clin Transl Sci*. 2014;7:82–86.
10. Hochhaus A, Kantarjian H. The development of dasatinib as a treatment for chronic myeloid leukemia (CML): from initial studies to application in newly diagnosed patients. *J Cancer Res Clin Oncol*. 2013;139:1971–1984.
11. Chen R, Chen B. The role of dasatinib in the management of chronic myeloid leukemia. *Drug Des Devel Ther*. 2015;9:773–779.
12. Hatori M, Ichinohasama R, Myers J, et al. Flow cytometric and genotypic analysis of primary non-Hodgkin's lymphoma of bone. *Pathol Res Pract*. 1997;193:557–564.
13. Kurita D, Miura K, Nakagawa M, et al. Dose-intensified CHOP with rituximab (R-Double-CHOP) followed by consolidation high-dose chemotherapies for patients with advanced diffuse large B-cell lymphoma. *Int J Hematol*. 2015;101:585–593.
14. Chao MP. Treatment challenges in the management of relapsed or refractory non-Hodgkin's lymphoma – novel and emerging therapies. *Cancer Manag Res*. 2013;5:251–269.
15. Daridon C, Blassfeld D, Reiter K, et al. Epratuzumab targeting of CD22 affects adhesion molecule expression and migration of B-cells in systemic lupus erythematosus. *Arthritis Res Ther*. 2010;12:R204.
16. Kato J, O'Donnell RT, Abuhay M, et al. Efficacy and toxicity of a CD22-targeted antibody-saporin conjugate in a xenograft model of non-Hodgkin's lymphoma. *Oncoimmunology*. 2012;1:1469–1475.
17. Morschhauser F, Kraeber-Bodéré F, Wegener WA, et al. High rates of durable responses with anti-CD22 fractionated radioimmunotherapy: results of a multicenter, phase I/II study in non-Hodgkin's lymphoma. *J Clin Oncol*. 2010;28:3709–3716.
18. Witzig TE, Tomblyn MB, Misleh JG, et al. Anti-CD22 90Y-epratuzumab tetraxetan combined with anti-CD20 veltuzumab: a phase I study in patients with relapsed/refractory, aggressive non-Hodgkin lymphoma. *Haematologica*. 2014;99:1738–1745.
19. Kuroda S, Tam J, Roth JA, et al. EGFR-targeted plasmonic magnetic nanoparticles suppress lung tumor growth by abrogating G2/M cell-cycle arrest and inducing DNA damage. *Int J Nanomedicine*. 2014;9:3825–3839.
20. Wang Y, Yi S, Sun L, et al. Charge-selective fractions of naturally occurring nanoparticles as bioactive nanocarriers for cancer therapy. *Acta Biomater*. 2014;10:4269–4284.
21. Wang J, Chen B, Chen J, et al. Synthesis and antitumor efficacy of daunorubicin-loaded magnetic nanoparticles. *Int J Nanomedicine*. 2011;6:203–211.
22. Wang J, Chen B, Chen J, et al. Apoptotic mechanism of human leukemia K562/A02 cells induced by magnetic iron oxide nanoparticles co-loaded with daunorubicin and 5-bromotetrandrin. *Int J Nanomedicine*. 2011;6:1027–1034.
23. Chen Z, Zhang Y, Xia J, et al. Preparation and characterization of water-soluble monodispersed magnetic iron nanoparticles via surface double-exchange with DMSA. *Colloids Surf A Physicochem Eng Asp*. 2008;316:210–216.
24. Sohn YS, Lee YK. Site-directed immobilization of antibody using EDC-NHS-activated protein A on a bimetallic-based surface plasmon resonance chip. *J Biomed Opt*. 2014;19:051209.
25. Munnier E, Cohen-Jonathan S, Linassier C, et al. Novel method of doxorubicin-SPION reversible association for magnetic drug targeting. *Int J Pharm*. 2008;363:170–176.
26. Sadighian S, Rostamizadeh K, Hosseini-Monfared H, et al. Doxorubicin-conjugated core-shell magnetite nanoparticles as dual-targeting carriers for anticancer drug delivery. *Colloids Surf B Biointerfaces*. 2004;117:406–413.
27. Gautier J, Munnier E, Paillard A, et al. A pharmaceutical study of doxorubicin-loaded PEGylated nanoparticles for magnetic drug targeting. *Int J Pharm*. 2012;423:16–25.
28. Reiter A, Schrappe M, Tiemann M, et al. Improved treatment results in childhood B-cell neoplasms with tailored intensification of therapy: a report of the Berlin-Frankfurt-Münster Group Trial NHL-BFM 90. *Blood*. 1999;94:3294–3306.

29. Oschlies I, Salaverria I, Mahn F, et al. Pediatric follicular lymphoma – a clinico-pathological study of a population-based series of patients treated within the Non-Hodgkin's Lymphoma-Berlin-Frankfurt-Münster (NHL-BFM) multicenter trials. *Haematologica*. 2010;95:253–259.
30. Pankhurst QA, Connolly J, Jones SK, et al. Applications of magnetic nanoparticles in biomedicine. *J Phys D Appl Phys*. 2003;36:R181.
31. Qiao R, Zeng J, Jia Q, et al. Magnetic iron oxide nanoparticle – an important cornerstone of MR molecular imaging of tumors. *Acta Phys Chim Sin*. 2012;28:993–1011.
32. Wu P, Li S, Zhang H. Design real-time reversal of tumor multidrug resistance cleverly with shortened carbon nanotubes. *Drug Des Devel Ther*. 2014;8:2431–2438.
33. Zaja F, Tomadini V, Zaccaria A, et al. CHOP-rituximab with PEGylated liposomal doxorubicin for the treatment of elderly patients with diffuse large B-cell lymphoma. *Leuk Lymphoma*. 2006;47:2174–2180.
34. Luminari S, Montanini A, Federico M. Anthracyclines: a cornerstone in the management of non-Hodgkin's lymphoma. *Hematol Rep*. 2011;3 (3 Suppl):e4.
35. Vaupel P. Tumor microenvironmental physiology and its implications for radiation oncology. *Semin Radiat Oncol*. 2004;14:198–206.
36. Tannock IF, Rotin D. Acid pH in tumors and its potential for therapeutic exploitation. *Cancer Res*. 1989;49:4373–4384.
37. Marina ML, Arlette GS, Berthold M, et al. How Fe^{3+} binds anthracycline antitumor compounds. The myth and the reality of a chemical sphinx. *J Inorg Biochem*. 1999;75:105–115.